We are IntechOpen,
the world's leading publisher of
Open Access books
Built by scientists, for scientists

4,800
Open access books available

122,000
International authors and editors

135M
Downloads

Our authors are among the

154
Countries delivered to

TOP 1%
most cited scientists

12.2%
Contributors from top 500 universities

BOOK CITATION INDEX
CLARIVATE ANALYTICS
INDEXED

WEB OF SCIENCE™

Selection of our books indexed in the Book Citation Index
in Web of Science™ Core Collection (BKCI)

Interested in publishing with us?
Contact book.department@intechopen.com

Numbers displayed above are based on latest data collected.
For more information visit www.intechopen.com

Investigation of High-Speed Transient Processes and Parameter Extraction of InGaAsP Laser Diodes

Juozas Vyšniauskas, Tomas Vasiliauskas, Emilis Šermukšnis,
Vilius Palenskis and Jonas Matukas
Vilnius University, Center for Physical Sciences and Technology,
Lithuania

1. Introduction

Fiber optic communication systems rely on the speed of the modulated light sources such as laser diodes (LDs). High speed direct current modulation of the optical signal, narrow spectral width, small dimensions and good light coupling efficiency to the optical fiber are the advantageous features of LD. Especially the long-haul optical links are critical to the chromatic dispersion and thus a single-mode and stable wavelength optical information carrier is needed. Distributed feedback (DFB) LDs are usually used in this situation. These DFB lasers have an almost single-mode optical emission spectrum, a stable optical frequency output, an optical modulation rate in excess of Gb/s and an uninterrupted operation time of up to 10^8 hours. However, the communication system with a high-speed direct modulation is limited by transient processes in the LD.

Optical links continually demand LDs with higher pulse modulation rates. Such techniques as eye diagrams, bit-error rate estimation, power penalty, pseudorandom bits sequences are used as the final and evident proof of LD suitability for specific link and speed applications. LDs with higher pulse modulation rate, higher extinction rate and optical power and also with a low chirp should be employed. Characterisation and modelling of LD dynamic characteristics is then needed. The investigation of small signal and large signal (pulse) characteristics can reveal the LD modulation speed in the fiber links and helps to better understand LD operation in other respects.

Rate equations for electron and photon densities in the active region of LD are widely used as a phenomenological model for the analysis of a small signal, a large signal and noise (Agrawal & Dutta, 1993; Agrawal, 2002; Fukuda, 1999). Despite the simplicity of the model, it predicts the modulation and noise of LD with good accuracy. It is also useful for LD characterisation and parameter extraction.

Small signal modulation equations in the frequency domain are derived directly from the rate equations assuming a small current perturbation at the given DC point. Thus, response spectra of optical power (or electron density) to the applied modulated current are analytically available. Parameters directly or indirectly entering rate equations and small signal modulation equations already comprise material and structural properties of LD. For

example, electron lifetime, photon lifetime in the LD cavity, differential gain, nonlinear gain K-factor are only a few parameters which are usually extracted from the small signal modulation measurements (Lu et. al., 1995).

In the case of relative intensity noise (RIN) analysis the situation is similar (Tatham et al., 1992). The similarity of both characterisations becomes obvious if one just notices that the difference is only in the modulation source acting on the same system (LD). First one is the external modulation source probing the response of the system and another one is an internal source of the origin of spontaneous fluctuations of the number of electrons and photons. One can recall the Fluctuation-Dissipation theorem which states that the response of the system at equilibrium to the external small signal perturbation is the same as the response to the spontaneously occurring fluctuations inside the system. However, one applies DC current and thus the system is not at equilibrium. But it means no more that an additional information in the fluctuation spectra could be present in principle. Quantitatively the precision of extracted parameters from RIN measurements should be lower compared with small signal modulation measurements due to the random nature of the detected signal. Qualitatively it may have advantages, since parasitic capacitances are avoided.

Another interesting point is that the equations for small signal modulation and RIN have minor differences in the cases of the LDs of different materials and even structures. One can compare the equations of conventional edge-emitting laser diode (studied here), vertical-cavity surface-emitting laser (VCSEL) (Larsson et. al., 2004) or even quantum-dot (QD) (Bhattacharya et. al., 2000) laser.

Here the case of large signal current modulation is studied. Given dynamic parameters of LD extracted from the small signal measurements (relative intensity noise (RIN) of the optical beam intensity) are compared with the parameters extracted from the large signal measurements (optical power and time-resolved frequency chirp). Contrary to the small signal, the rate equations do not have closed-form expressions for the solutions of large signal (pulse) and thus rate equations should be integrated numerically. If the small signal parameter extraction from the experimental results consists of the standard function fitting procedure, then due to the lack of the closed-form function (in the case of a large signal) one needs other fitting means.

In this work rate equations were numerically solved taking the fixed set of input parameters such as the lifetime of photons, the coefficient of optical amplification, the nonlinear amplification factor, the spontaneous radiation and the optical confinement factor etc. The numerical solution obtained is then compared with the pulse from experiment. The procedure is repeated with a different set of parameters until the best coincidence is obtained. The final results of simulation were compared with experimental ones and the matching accuracy was calculated

2. Large signal: Optical power modulation and chirp

In the time domain, the small signal solutions of the rate equations are in the form of decaying oscillations (oscillation-relaxation solutions) in the densities (or number) of electrons and photons. After a small disturbance, coupled subsystems of electrons and photons oscillate (in number), exchange and dissipate the energy while approaching stationary conditions until the next disturbance. Two terms appear: the oscillation-relaxation frequency (showing the rate of exchange) f_0 and the damping frequency (showing the rate of dissipation) Γ_0. In the frequency domain this process has the form of resonance spectrum.

In the case of a large signal (pulse modulation) oscillation-relaxation rings form after the leading and trailing edges of the rectangular pulse. Thus, the pulsed bias current modulates the number of electrons and photons in the active region of LD (Agrawal & Dutta, 1993). The number of photons is proportional to the lased optical power (Agrawal & Dutta, 1993). which can be measured. The pulsing number of electrons is responsible for the frequency chirp phenomena inherent to LDs. The chirp is a considerable change in the frequency (wavelength) of the optical mode of the LD during the large signal modulation. This frequency chirp can also be measured. The origin of this effect relates to the other phenomena present even at the continuous-wave (cw) operation of LD. It manifests in the enhanced linewidth of the optical mode of the LDs. The principle of that is a change in the real and imaginary parts of the refractive index n' and n'' as electron density is pulsing (chirp) or fluctuates (linewidth enhancement). The phenomenon and the linewidth enhancement factor (or chirp parameter) $a = \Delta n' / \Delta n''$ showing the intensity of the phenomenon itself were correspondingly explained and introduced by C. H. Henry (Henry, 1982, 1983, 1986). Measurements of the frequency chirp during large signal modulation is a well-known technique for the estimation of the optical signal transmission in the fiber communications. The chirp intensity is proportional to the electron density, and thus also features oscillation-relaxation behaviour during the pulse modulation. This can be seen in the time-resolved frequency chirp measurements.

There are several chirp parameter extraction methods and the time-resolved chirp method is one of them (Harder et al., 1983; Arakawa & Yariv, 1985; Kikuchi et al., 1984; Kikuchi & Okoshi, 1985; Linke, 1985; Bergano, 1988). In fact, this method is more frequently used for electro-optical modulators, where the time-resolved chirp is a little simpler than that of LD, because there is only a transient term (Jeong & Park, 1997). Time-resolved frequency chirp measurements reveal more detailed information about LDs optical beam frequency behaviour by comparing with ordinary averaged optical beam spectrum measurements, because the time-resolved representation of frequency deviations shows specific chirp details, such as frequency oscillations and the amplitude of these oscillations (Welford, 1985; Olsen & Lin, 1989; Tammela et al., 1997).

2.1 Devices under investigation

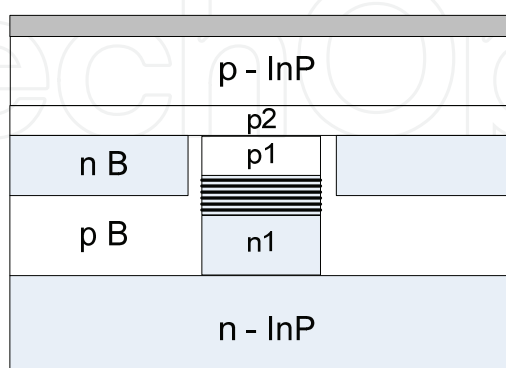A schematic diagram of the finished laser structure (around the mesa) is shown in Fig. 1.

Fig. 1. Schematic diagram of the finished laser structure in the vicinity of the mesa. p-InP p:10^{18} cm^{-3}, p2-InP p:10^{18} cm^{-3}, p1-InP p:$5 \cdot 10^{17}$ cm^{-3}, n1-InP n:10^{18} cm^{-3}, n -InP n:10^{18} cm^{-3} nB-InP n:10^{18} cm^{-3}, pB-InP p:$6 \cdot 10^{17}$ cm^{-3}. Active region of the InGaAsP MQWs is formed between p1 and n1 layers.

The laser structure is epitaxially grown on (100) oriented n-doped InP substrates. The residual reflectivity of the front facet coating is within 3 to 8% as measured at the lasing wavelength. The rear facet is coated with a high reflectivity coating of 60 to 80%.

The active region of the investigated laser diodes is buried between two side layers which helps to make the active region bounded in transversal direction. Six strained quantum wells are formed in the active region. In addition, there are periodically truncated quantum wells along the longitudinal axis of the active region, which helps to create a periodical refractive index (due to different refractive indexes of the material in the truncating region) and a periodical optical gain (due to non-uniform carrier density); that forms gain-coupled (plus index-coupled) distributed feedback.

2.2 Time-resolved frequency chirp measurement setup and methodology

Time-resolved frequency chirp measurements setup under pulse operation is shown in Fig. 2. LD bias current is modulated by using a rectangular pulse generator together with a direct current source connected through the wideband bias tee. When the bias current was modulated, the optical beam power and optical wavelength became modulated as well. The optical beam is coupled to the tapered fiber (Shani et al., 1989; Alder et al., 2000), which is connected to a Mach-Zehnder fiber interferometer (Saunders et al., 1994; Jeong & Park, 1997; Laverdiere et al., 2003). An optical amplifier can be used if the interferometer output signal is too weak. Then an optical signal is passed to an optical input of the sampling oscilloscope connected to the PC. The most important part of the setup is the automated Mach-Zehnder fiber interferometer (Fig. 2). The main advantages of the interferometer are a quick time-domain chirp measurement, which takes only 30 seconds or less, high-resolution (< 20 MHz) and high measurement frequency (50 GHz or more). This allows to measure transmission signals greater than 10 Gbps with the measurement repeatability of ~5%.
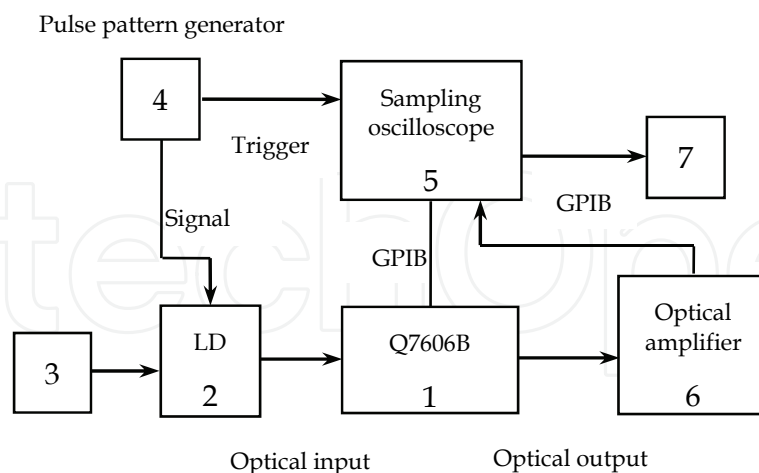
Fig. 2. Chirp measurement setup. (1) Mach-Zehnder fiber interferometer (Advantest Q7606B Optical Chirpform Test Set), (2) semiconductor laser, (3) direct current source (ILX Lightwave LDC–3900 modular laser diode controller), (4) pulse pattern generator (Agilent HP-70843B error performance analyzer), (5) signal analyzer – digital sampling oscilloscope (Tektronix TDS8000 Digital Sampling Oscilloscope), (6) erbium doped fiber amplifier, (7) personal computer with integrated General Purpose Interface Bus (GPIB) interface

An automated polarization controller helps to fix optimal polarization direction. That increases measurement accuracy. By changing the optical path delay time the interferometer can automatically fit the frequency transfer function to a particular carrier frequency of optical signal. The frequency transfer function of the Mach-Zehnder fiber interferometer is shown in Fig. 3. As can be seen, it is a sinusoidal function and its period is called a free spectral range (FSR). The optical signal frequency (chirp) variation should be lower than FSR/4=35 GHz. The frequency transfer function can be arbitrarily shifted with respect to the optical signal carrier frequency. And thus, during the first phase the frequency transfer function is shifted to the carrier frequency at the point "A", during the second phase – at the point "B" Fig. 3.

The frequency transfer function can be written as:

$$K_{total} = \beta K(f) = \beta \frac{A}{2} \cos\left(\frac{2\pi f}{FSR} \right) . \tag{1}$$

where β is a optical loss in the system and A is amplitude of transfer function.

It follows from the equation (1) that the transfer coefficient depends on carrier frequency. During the pulse modulation the carrier frequency varies in time as:

$$f(t) = f_{cw} + \Delta f(t) . \tag{2}$$

The last term in equation (2) is a frequency chirp. At first, in order to measure the chirp of the LD or any other device, the optical beam should be passed to the interferometer not modulated, so that the carrier frequency and optical power should be constant. Then the carrier frequency is f_{cw}. As was mentioned earlier, the transfer function is shifted to match f_{cw} to the point "A" and after – to the point "B".
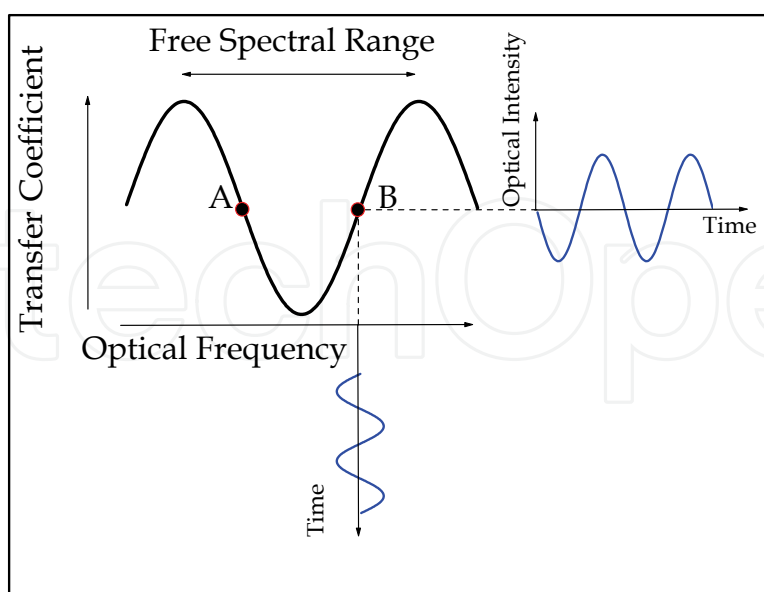

Fig. 3. Mach-Zehnder interferometer frequency transfer function

In both cases the transfer function will be shifted and the transfer coefficient will depend on $\Delta f(t)$.

$$K_A = \beta \left[\frac{A}{2} + \frac{A}{2} cos \left(\frac{2\pi\Delta f}{FSR} \right) \right] , \tag{3}$$

$$K_B = \beta \left[\frac{A}{2} - \frac{A}{2} cos \left(\frac{2\pi\Delta f}{FSR} \right) \right] . \tag{4}$$

Thus the output signal power in both cases is:

$$P_{outA}(t) = P_{in}(t)\beta \left[\frac{A}{2} + \frac{A}{2} cos \left(\frac{2\pi\Delta f(t)}{FSR} \right) \right] , \tag{5}$$

$$P_{outB}(t) = P_{in}(t)\beta \left[\frac{A}{2} - \frac{A}{2} cos \left(\frac{2\pi\Delta f(t)}{FSR} \right) \right] . \tag{6}$$

In literature these two equations are usually called IM+FM and IM-FM, because in both of them there are two terms which correspond to power modulation and frequency modulation (chirp). So, in both measurement phases (points "A" and "B") the output power depends not only on the chirp but on the input signal power as well. However, after both measurements are done, the power modulation term can be cancelled:

$$\frac{P_{outA}(t) - P_{outB}(t)}{P_{outA}(t) + P_{outB}(t)} = cos \left(\frac{2\pi\Delta f(t)}{FSR} \right) = P_{calc}(t) . \tag{7}$$

There $P_{calc}(t)$ only contains information about chirp (carrier frequency deviations) but there is no information about power deviations. Further, the chirp can be easily obtained:

$$\Delta f(t) = \frac{FSR}{2\pi} arccos \left(P_{calc}(t) \right) . \tag{8}$$

Or, in case when $\Delta f(t)$<<FSR/4, cosine can be treated as a line and the equation (8) becomes:

$$\Delta f(t) = \frac{FSR}{2\pi} P_{calc}(t) . \tag{9}$$

In fact, the LD length is only 300 μm, so in order to make various measurements handily the LD needs to be put on some device carrier (Fig. 4). The device carrier is useful to easily connect a coaxial microwave probe because the LD is located on the microwave microstrip line. There is a serial resistor implanted in the microstrip line in order to match the microstrip line and LD impedances, so that the reflected parasitic signals are cancelled. The microwave cable is connected to a microstrip line by using the microwave probe (RF probe). The cut-off frequency of the microwave probe is ~ 50 GHz. For high frequency measurements any other DC interfaces composed of any LRC circuits should be disconnected.

The detected signal at the optical input of the oscilloscope is quite noisy Fig. 5. The optical pulse is attenuated and cumulates enough noise while it propagates throughout the system. Noise types and sources are different. There is a white amplitude noise, which continuously distributes through the length of the pulse; there is also a phase noise or jitter, which appears

because the pulse length or the beginnings of the pulse edges fluctuates. The fiber interferometer and the scope also contribute to the noise level. As was explained, the output signal of the Mach-Zehnder interferometer is displayed on the digital scope screen as well as in the scope's internal memory. It is possible to make inter sample averaging (ensemble averaging); the scope can average up to 1024 samples. That possibility is very important for the periodic signal, because it helps to increase the S/N (signal to noise ratio) (no noise in Fig. 6).
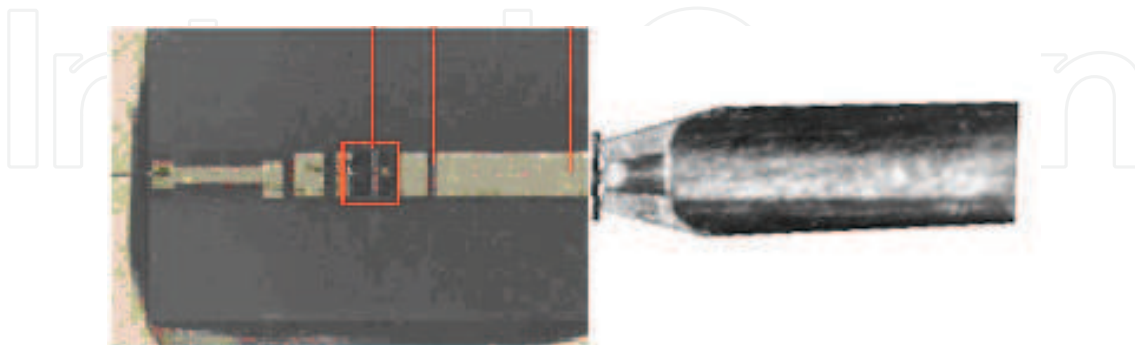

Fig. 4. LD ceramic carrier together with LD, microstrip line and a microwave probe on it
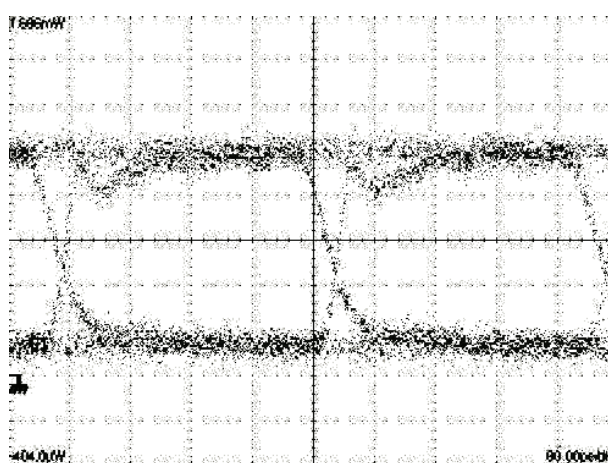

Fig. 5. Eye diagram of a not averaged (noisy) pulse train
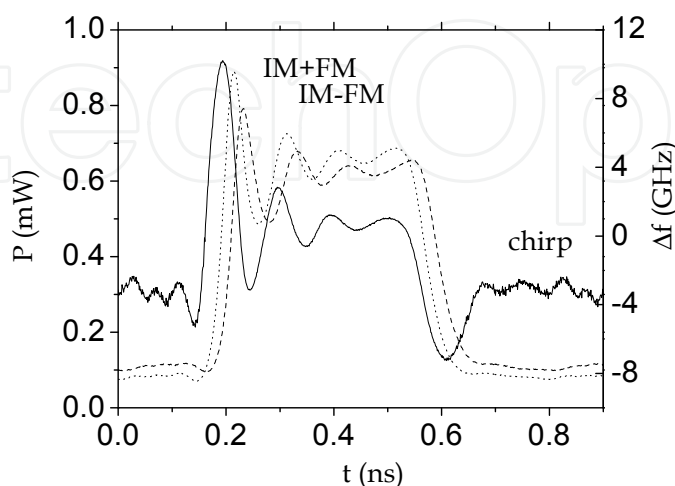

Fig. 6. Chirp pulse plotted together with interferometer output pulses corresponding to both frequency transfer function points

Another effective method is a software high frequency filtering with f_c=50 GHz which should be applied to the already averaged signal in the scope's memory. Such a filter is admissible because the cut-off frequency of the microwave system is also ~50 GHz, and so, all higher frequencies could be considered as parasitic.

After all these noise-related measurement problems were resolved, it became possible to make high-quality time-resolved chirp measurements. After both power pulses IM+FM and IM-FM were measured, by using the equation (9), the chirp pulse was obtained. All three pulses are shown in Fig. 6.

2.3 Time-resolved frequency chirp measurement results

A typical chirp pulse is shown in Fig. 7a, which is referred to as total chirp. The relatively plain region in the chirp waveform is referred to as adiabatic chirp and oscillations (blue or red shifts) corresponding to both power pulse edges are referred to as transient chirp. There the total chirp is the actually observed chirp, which can be expressed as the sum of transient and adiabatic chirp. While the pulse form of the adiabatic chirp is the same as the form of the optical power pulse, the transient chirp is proportional to the optical power derivative (derivative of ln(P) (Kikuchi, 1990; Koyama & Suematsu, 1985):

$$\Delta f(t) = \frac{a}{2\pi}\left[\frac{\dot{P}(t)}{P(t)} + G_P P(t)\right],$$ (10)

where P is the photon number, G_P is the nonlinear gain, α is the chirp parameter. The chirp parameter affects both the transient and the adiabatic chirp, while the nonlinear gain affects only the adiabatic chirp (equation (10)). The presence of the adiabatic term distinguishes the LD from the electro-optical modulators (EOM) due to nonlinear gain (Jeong & Park, 1997). While the electro-optical modulator chirp has only a transient part, the LD chirp has a transient and an adiabatic term (Fig. 7).
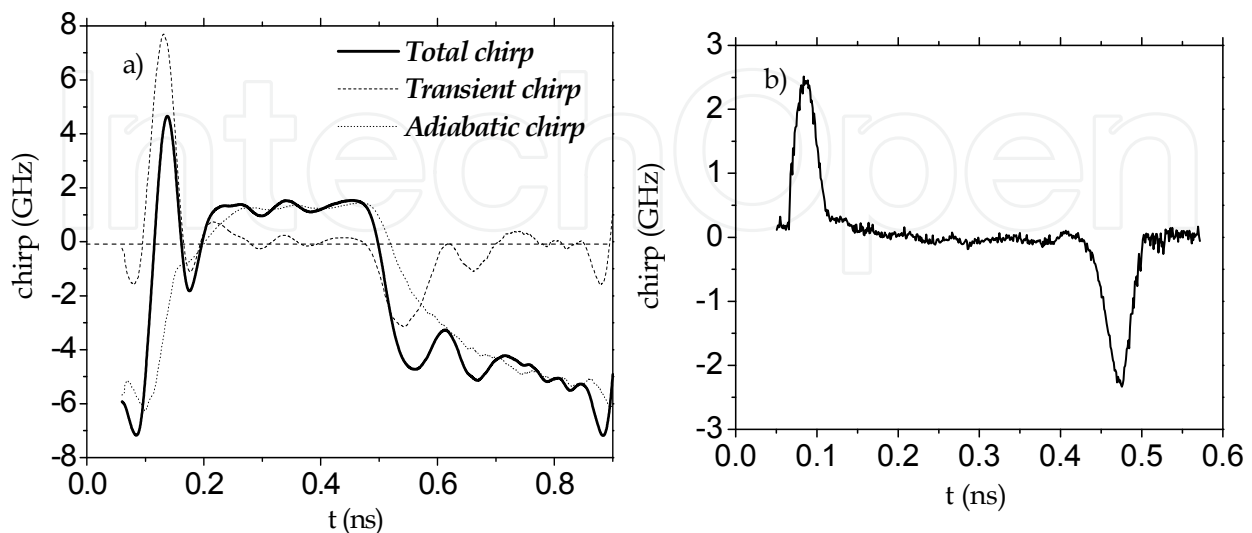

Fig. 7. LD time-resolved frequency chirp waveform of LD a) (Šermukšnis et al., 2005) and electro-optical modulator b)

The chirp pulse can be further used for LD analysis. Chirp and power pulses are shown below in Figs. 8a and 9a. The chirp pulse begins earlier than the power pulse, thus there is some time or phase shift between them. As current pulse is applied, the optical beam carrier frequency (as well as the wavelength) starts to change but the power still stays constant. The chirp parameter is extracted from both measured pulses, as explained in detail below.
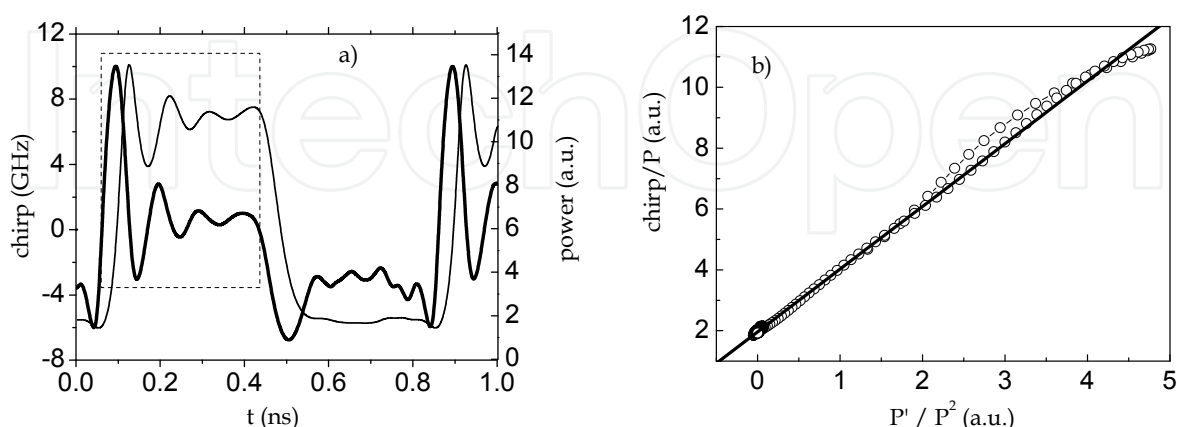

Fig. 8. Chirp parameter extraction in case of a 2.5 Gbit/s modulation rate. Frequency chirp and optical beam power waveform a), linearised time-resolved frequency chirp waveform b) (Šermukšnis et al., 2005)
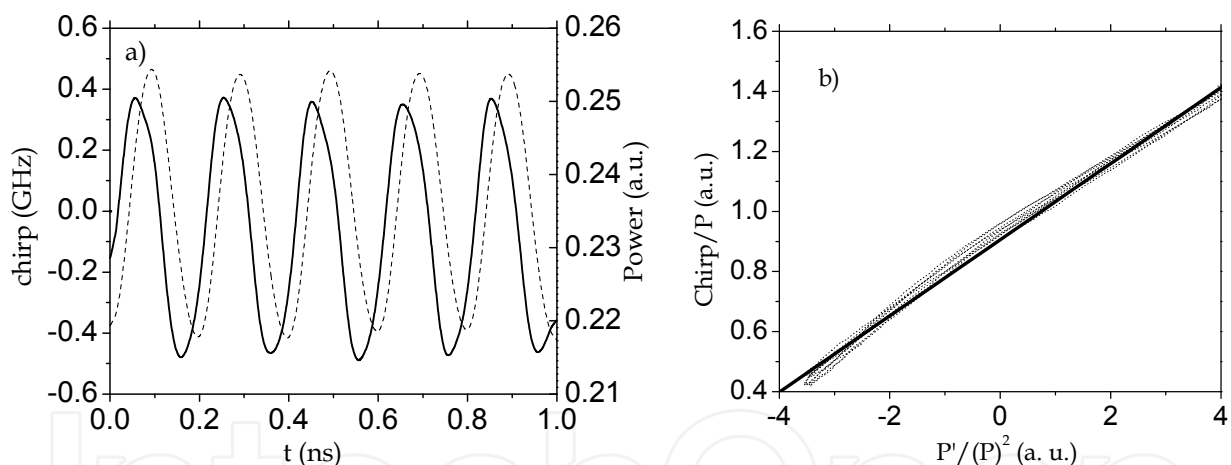

Fig. 9. Chirp parameter extraction in case of a 10 Gbit/s modulation rate. Frequency chirp and optical beam power waveform a), linearised time-resolved frequency chirp waveform b) (Šermukšnis et al., 2005)

In optoelectronic devices such as LDs or electro-optical modulators the chirp parameter should preferably be small. Besides, the chirp parameter extraction with good accuracy is not always possible. Dividing both sides of the equation (10) by the photon number P and after plotting $\Delta f / P$ versus $\dot{P} / P^2$, linear dependence of these two terms is expected. It was observed that in most cases such linear dependence actually occurs, furthermore, the linearity is of good quality (Figs. 8b and 9b). From the slope of that linear plot, the chirp parameter can be extracted. Considering that the photon number is proportional to the optical beam power P_W, the term $\dot{P} / P$ in the equation (10) is equal to $\dot{P}_W / P_W$. So, in real experiment conditions not the photon number P but the optical beam power P_W was used.

For simplicity and accuracy, only part of the single pulse, which is shown in Fig. 8a (area in the dash square), was taken for chirp parameter extraction. The other part of the pulse has a considerable noise and distortion at the „0" level of the chirp pulse. Better accuracy is also reached when a 10 Gbit/s bias current pulse sequence is generated and the corresponding chirp waveform is used (Fig. 9). There, in Fig. 9b, good linearity, as well as good chirp parameter extraction precision, can obviously be seen. Though bias current pulses were almost of rectangular form, as can be seen in Fig. 9a, both power and chirp pulses are of semi-sinusoidal form. Of course, that occurs when the modulation rate becomes comparable to the LD direct current modulation speed limits. By comparing these two cases it was observed that the chirp parameter extraction error does not exceed 10 %. Several tens of lasers were measured in such manner and the chirp parameter for all of them was extracted. It was found that this parameter of these lasers is dispersed between 2 and 2.8.

Besides the chirp parameter, time-resolved chirp pulse amplitude is also important. As it was shown above, there are large damped oscillations at the leading and trailing edges of both power and chirp pulses Figs. 8a and Fig. 10b. At a high modulation rate, these oscillations can increase several times, so that the ring amplitude becomes considerably larger than the distance between „1" and „0" levels. In that case, the rings comprise the large part of the total chirp, as well as have the considerable effect on the pulse propagation in the fiber.
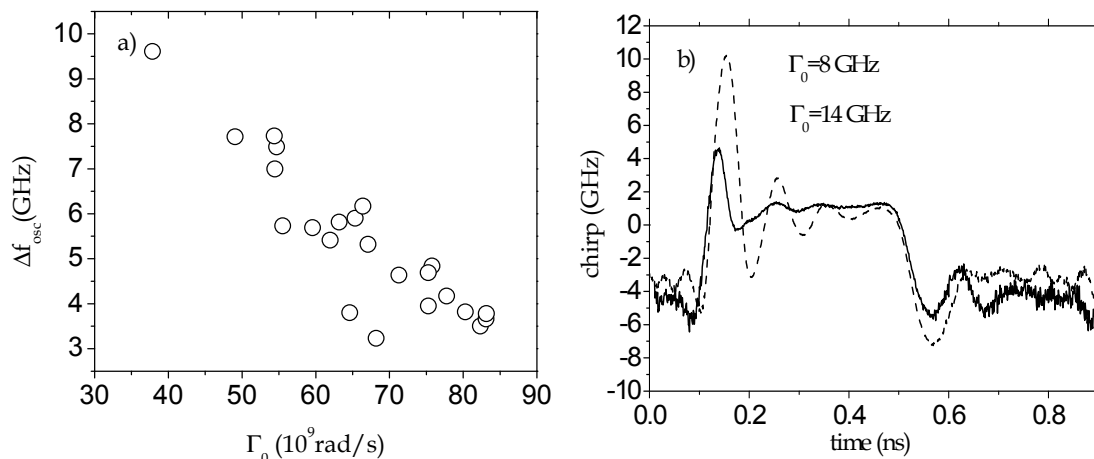
Fig. 10. Chirp pulse ring amplitude dependence on damping rate a) (Šermukšnis et al., 2005) and chirp pulse comparison for two lasers with different damping rate b)

It is always desirable to have chirp rings smaller, particularly in these cases, when rings make the largest contribution to the pulse power. In order to find the chirp ring amplitude analytically, one should account for many factors. Besides, the analytical analysis of a large signal is especially complicated. The oscillation frequency and the oscillation amplitude damping rate nearly correspond to the oscillation-relaxation and damping frequency which are used in small signal analysis. Indeed, it was observed that the amplitude (amplitude of the first ring, which largely contributes to the transient chirp) and the damping rate of chirp rings strongly depends on a small signal damping frequency (extracted from RIN measurements) at constant power for different LDs (Fig. 10). It is smaller in lasers with a large damping rate (Fig. 10b).

To summarise, the adiabatic chirp of different LDs was in the region of 4.2 GHz to 5.6 GHz and the dynamic chirp in the region of 3.2 GHz to 10 GHz. Finally, it was observed that in

regular direct current modulation conditions the frequency chirp variation does not exceed 16 GHz in average. For a semiconductor laser with the wavelength of 1550 nm, that corresponds only to about ~0.1 nm variation in wavelength. Such wavelength variation compared to the total wavelength 1550 nm is negligible but even such small variation can noticeably affect the optical pulse propagation in the optical fiber due to chromatic dispersion, particularly when the data transmission rate is high.

3. Theoretical models

In this work four physical models were used. At first, a simplified physical model based on rate equations for carrier and photon densities was used for computer simulation (Šermukšnis et al., 2004a, 2004b). However, though some of the physical factors were not included in this model, the accuracy of modelling results for some DFB lasers was sufficiently good. In the later models, the rate equations were supplemented with additional physical parameters.

For the second physical model the nonlinear amplification factor ε was included in the rate equations. The optical amplification coefficient, α [cm³/s] was assumed to be equal to the product of the optical differential amplification, g [cm²], and the group velocity, v_g ($\alpha = v_g g$) in the earlier model of simplified rate equations (Šermukšnis et al., 2004a, 2004b). Including that the optical amplification depends on the photon density:

$$g(N,P) = g_0(1 - \varepsilon P) = g(N - N_0)(1 - \varepsilon P),\qquad(11)$$

where N is the density of electrons, P is the density of photons, N_0 is the carrier density at transparency (corresponding to the onset of population inversion) and ε is the nonlinear amplification factor. Then the term of the number of photons generated by spontaneous emission in the rate equations was supplemented with the factor $(1 - \varepsilon P)$.

In the third model, the term N/τ_s in the rate equation (Šermukšnis et al., 2004a, 2004b) is changed to $N\gamma_e(N)$, because $\gamma_e = 1/\tau_s$, where $\gamma_e(N)$ is the rate of electron recombination (Carroll et al., 1998):

$$\gamma_e(N) = A + BN + CN^2,\qquad(12)$$

where the first term A of the equation describes the non-radiative recombination, B is the coefficient of radiant interband recombination and C is the coefficient of Auger recombination. The carrier lifetime τ_s can be described by these parameters in such a way:

$$\tau_s(N) = (A + BN + CN^2)^{-1},\qquad(13)$$

and can be used in the rate equations (14).

In the fourth model we used the following rate equation for electron density (Carroll et al., 1998):

$$\frac{dN}{dt} = \frac{J}{ed} - N(A + BN + CN^2) - a(N - N_0)(1 - \varepsilon P)P,\qquad(14)$$

where J is the density of injection current, e is the electron charge, d is the width of the semiconductor laser active region, t is the time. The first term of the rate equation (14) describes the number of injected carriers that passed the unit volume per unit time interval, the second one describes the spontaneous emission and the third term defines the number of photons generated by stimulated emission per unit time interval. An analogical equation was used for photon density:

$$\frac{dP}{dt} = \Gamma a (N - N_0)(1 - \varepsilon P) P - \frac{P}{\tau_p} + \Gamma \beta B N^2 , \tag{15}$$

where τ_p is the lifetime of photons, β is the spontaneous emission factor, Γ is the optical confinement factor. The first term of the rate equation (15) is the number of photons generated by stimulated emission per unit time interval, the second term is the number of photons emitted from a resonator (output of the laser). The third term of the equation (15) shows the spontaneous emission contribution to the generated mode.

4. Used experimental results

Experimental results of DFB semiconductor lasers were used for computer simulation. Not all laser parameters needed for simulation were known and some parameters were estimated from experimental results. The product of photon and electron lifetimes, the threshold current and the current at the 5 mW average optical power were known. The extinction ratio (ratio of the optical power level "1" to the level "0") was equal to 8.5 dB:

$$10 \lg (P_1 / P_0) = 8.5 . \tag{16}$$

Injection current values at levels "0" and "1" were found from the optical power dependence on injected current by using the condition (6) for the optical power of 5 mW. The active region width was estimated from the TEM image. We also had a possibility to calculate the injection current density from current measurements.

The experimentally obtained parameters of semiconductor DFB lasers, which were used for calculations (see Figs. 11-15):

- product of lifetimes, $\tau_s \tau_p$ (different for each laser);
- threshold current, I_{th} (different for each laser);
- mean current (current, when the average optical power is equal to 5 mW), I_{op} (different for each laser);
- optical powers: $P_1 = 8.59$ mW; $P_0 = 1.41$ mW (the same for all lasers);
- injection currents: I_1 (level „1") and I_0 (level „0"), found from the optical power dependence on injected current (see Fig. 11);
- dimensions of the active region of the DFB laser: $L = 300$ μm (channel length); $w = 1.5$ μm (width); $d = 0.1$ μm (thickness); $S = L \cdot w = 4.5 \cdot 10^{-6}$ cm² (area) (the same for all lasers);
- injection current density (calculated by using active region dimensions);
- experimental pulse characteristics: optical power and chirp (different for each laser).

These experimental results for all investigated lasers are shown in Table 1.

No.	DFB laser	$\tau_s\tau_p$ [s²]	I_{th} [mA]	I_{op} [mA]	J_{th} [A/cm²]	J_1 [A/cm²]	J_0 [A/cm²]
1.	O6j5	1.91·10⁻²⁰	12.31	33.09	2736	10711	4066
2.	H3k7	1.63·10⁻²⁰	11.56	33.07	2569	10756	3958
3.	G3k4	1.64·10⁻²⁰	11.89	32.94	2642	10638	3982
4.	J5k7	1.65·10⁻²⁰	11.15	34.26	2478	11300	3927
5.	U2i3	2.26·10⁻²⁰	8.19	30.10	1820	10184	3282
6.	R4j5	1.72·10⁻²⁰	11.29	32.33	2509	10542	3827
7.	E3k4	1.68·10⁻²⁰	11.36	34.38	2524	11313	3967
8.	G1l1	1.60·10⁻²⁰	11.74	32.80	2609	10649	3929
9.	P5i3	2.12·10⁻²⁰	8.72	30.65	1938	10309	3311
10.	T2s2	2.06·10⁻²⁰	8.85	31.46	1967	10767	3449
11.	S2i3	2.37·10⁻²⁰	8.09	28.94	1798	9758	3104
12.	R2r3	1.72·10⁻²⁰	11.44	35.80	2542	11842	4069
13.	T2i3	2.25·10⁻²⁰	8.02	31.63	1782	10796	3262
14.	Q1t1	1.62·10⁻²⁰	11.12	36.82	2471	12282	4082
15.	O1k1	1.63·10⁻²⁰	10.50	35.32	2333	11809	3871
16.	O2s2	1.99·10⁻²⁰	8.74	32.34	1942	10951	3389

Table 1. Experimental results used for simulation (Vasiliauskas et al., 2007)

5. Simulation results

Computer simulation was based on the fourth-order Runge-Kutta method for the system of differential equations. The values of photon and electron densities for different time moments were found from initial values of densities, determining other parameters and choosing the time step and the number of calculation loops.
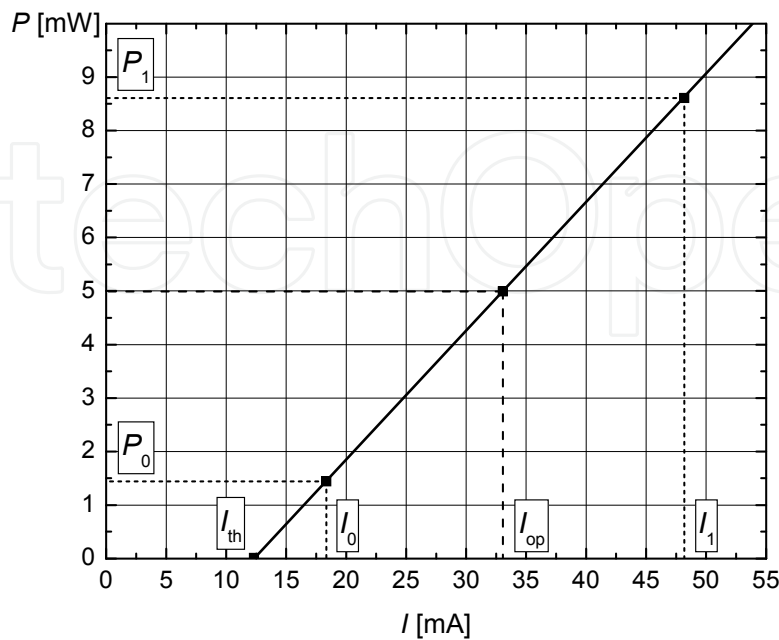

Fig. 11. Optical power dependence on injection current (Vasiliauskas et al., 2007)

In the computer simulation the following unknown parameters were selected: the optical confinement factor Γ, the reflection coefficients from mirrors at the ends, R_1 and R_2 (Fukuda, 1999), the lifetime of photons, τ_p, the coefficient of optical amplification, α, the spontaneous emission factor, β, the carrier density at transparency, N_0, the nonlinear amplification factor, ε, and the coefficients of recombination A, B and C.

The investigation of laser parameter interplay was done. Based on the simulation results obtained, the following technique for the estimation of semiconductor laser parameters was suggested:

- the frequency of the relaxation oscillation is defined by changing the coefficient of optical amplification, a;
- the calculated optical power values are approached to the experimental ones by changing the optical confinement factor Γ;
- by changing the nonlinear amplification factor, ε_1, and the spontaneous emission factor, β, the relaxation oscillation amplitudes can be corrected; in addition, the shape of oscillations can also be corrected by changing the injection current front duration;
- the recombination coefficient, A, and the density of electrons at transparency, N_0, was changed to optimize the static characteristics of the semiconductor laser;
- the recombination coefficients B and C were chosen last. These coefficients have insignificant influence on laser dynamics, they only change the shape of the oscillations a little.

The calculations for model verification were done, one of them being the investigation of watt-ampere characteristics (see Fig. 12). The threshold current was found as well. The results obtained were also compared to those of other authors (Agrawal & Dutta, 1993).
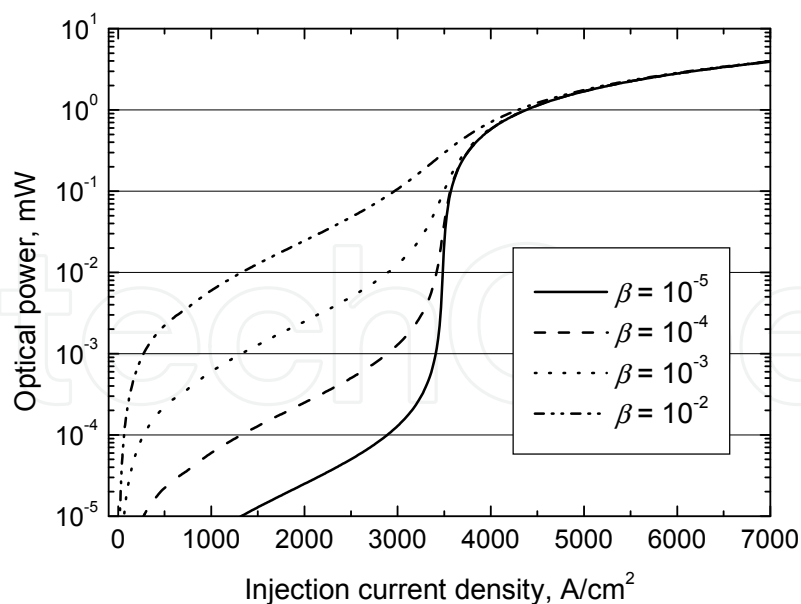

Fig. 12. Watt-ampere characteristics of a laser diode near the threshold of injection current for different spontaneous emission factors β (Vasiliauskas et al., 2007)

The output optical power of the semiconductor laser was calculated by using these equations (Agrawal & Dutta, 1993):

$$P_1 = \frac{hc^2}{\lambda \mu_g} \frac{1}{2L} log \frac{1}{R_1 R_2} L dw n_{ph} \frac{(1-R_1)R_2^{1/2}}{\left(R_1^{1/2}+R_2^{1/2}\right)\left(1-R_1^{1/2}R_2^{1/2}\right)},$$ (17)

$$P_2 = \frac{hc^2}{\lambda \mu_g} \frac{1}{2L} log \frac{1}{R_1 R_2} L dw n_{ph} \frac{(1-R_2)R_1^{1/2}}{\left(R_1^{1/2}+R_2^{1/2}\right)\left(1-R_1^{1/2}R_2^{1/2}\right)},$$ (18)

where R_1 and R_2 are the reflection coefficients of end mirrors, h is the Planck's constant, c is the speed of light, λ is the wavelength of radiated light, μ_g is the group refraction index, L is the length of the laser active region, d is the thickness of the active region, w is the active region width and n_{ph} is the density of photons.

The best results were obtained based on the fourth physical model (equations (14) and (15)). The most precise match of experimental and simulation results for all investigated lasers with different characteristics was obtained. The mismatch of analyzed laser parameters does not exceed the limit of 10%.
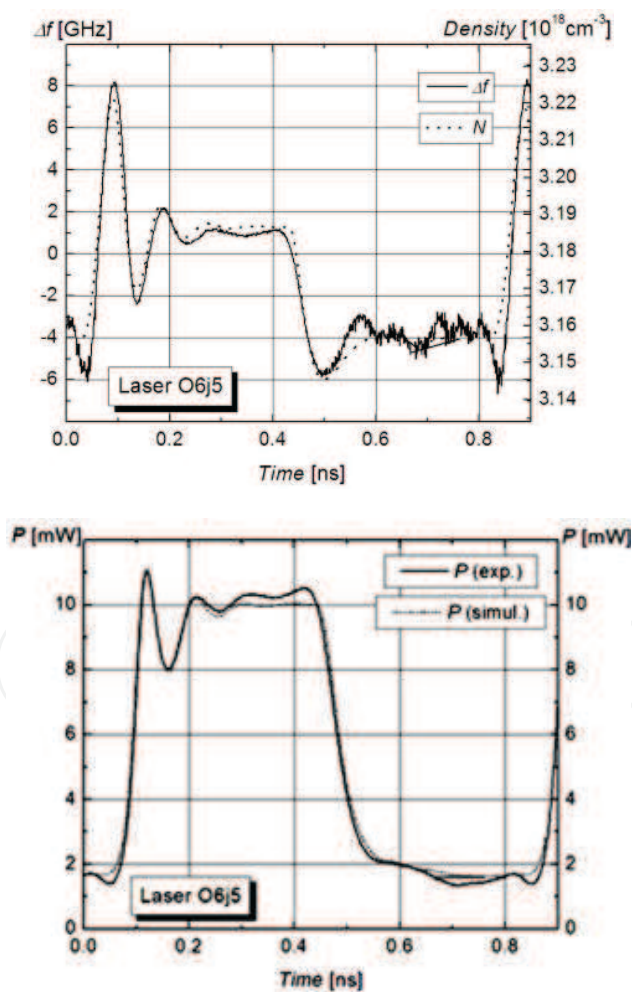

Fig. 13. Simulated electron density (N) and experimental chirp (Δf) pulse characteristics (Vasiliauskas et al., 2007) a), and experimental P(exp.) and simulated pulse characteristics P(simul.) of optical power (Vasiliauskas et al., 2007) b)

No.	DFB laser	Γ	R_1	R_2	τ_p [ps]	α [cm³/s]	β	N_0 [cm⁻³]
1.	O6j5	0.55	0.04	0.664	1.5	$16.8 \cdot 10^{-7}$	$1 \cdot 10^{-4}$	$24.3 \cdot 10^{17}$
2.	H3k7	0.49	0.08	0.80	2.0	$24.2 \cdot 10^{-7}$	$1 \cdot 10^{-3}$	$27.0 \cdot 10^{17}$
3.	G3k4	0.49	0.08	0.80	2.0	$23.6 \cdot 10^{-7}$	$1 \cdot 10^{-3}$	$27.0 \cdot 10^{17}$
4.	J5k7	0.33	0.08	0.80	3.0	$29.6 \cdot 10^{-7}$	$1 \cdot 10^{-3}$	$26.0 \cdot 10^{17}$
5.	U2i3	0.37	0.08	0.80	2.0	$21.6 \cdot 10^{-7}$	$1 \cdot 10^{-4}$	$14.0 \cdot 10^{17}$
6.	R4j5	0.67	0.08	0.80	1.8	$21.0 \cdot 10^{-7}$	$1 \cdot 10^{-2}$	$25.0 \cdot 10^{17}$
7.	E3k4	0.32	0.08	0.80	3.4	$29.0 \cdot 10^{-7}$	$1 \cdot 10^{-3}$	$27.0 \cdot 10^{17}$
8.	G1l1	0.42	0.08	0.80	3.0	$26.0 \cdot 10^{-7}$	$1 \cdot 10^{-2}$	$28.0 \cdot 10^{17}$
9.	P5i3	0.61	0.08	0.80	2.0	$20.0 \cdot 10^{-7}$	$1 \cdot 10^{-2}$	$23.0 \cdot 10^{17}$
10.	T2s2	0.57	0.08	0.80	1.5	$17.0 \cdot 10^{-7}$	$1 \cdot 10^{-3}$	$19.0 \cdot 10^{17}$
11.	S2i3	0.38	0.08	0.80	1.9	$22.0 \cdot 10^{-7}$	$1 \cdot 10^{-3}$	$17.0 \cdot 10^{17}$
12.	R2r3	0.66	0.08	0.80	2.1	$19.0 \cdot 10^{-7}$	$1 \cdot 10^{-3}$	$24.0 \cdot 10^{17}$
13.	T2i3	0.41	0.08	0.80	2.0	$29.0 \cdot 10^{-7}$	$1 \cdot 10^{-2}$	$15.0 \cdot 10^{17}$
14.	Q1t1	0.31	0.08	0.80	2.3	$29.0 \cdot 10^{-7}$	$1 \cdot 10^{-2}$	$25.0 \cdot 10^{17}$
15.	O1k1	0.48	0.08	0.80	2.5	$26.0 \cdot 10^{-7}$	$1 \cdot 10^{-2}$	$29.0 \cdot 10^{17}$
16.	O2s2	0.35	0.08	0.80	1.9	$28.0 \cdot 10^{-7}$	$1 \cdot 10^{-3}$	$28.0 \cdot 10^{17}$

Table 2. Fourth model: computer simulation results (1) (Vasiliauskas et al., 2007

No.	DFB laser	ε	τ_{j1} [ps]	τ_{j2} [ps]	A [cm/s]	B [cm³/s]	C [cm⁶/s]
1.	O6j5	$9.5 \cdot 10^{-18}$	54	50	$2.5 \cdot 10^8$	$9.1 \cdot 10^{-12}$	$3.80 \cdot 10^{-29}$
2.	H3k7	$11 \cdot 10^{-18}$	56	53	$2.8 \cdot 10^8$	$8.4 \cdot 10^{-12}$	$3.25 \cdot 10^{-29}$
3.	G3k4	$11 \cdot 10^{-18}$	56	53	$2.8 \cdot 10^8$	$8.4 \cdot 10^{-12}$	$3.25 \cdot 10^{-29}$
4.	J5k7	$15 \cdot 10^{-18}$	50	50	$3.6 \cdot 10^8$	$4.7 \cdot 10^{-12}$	$2.44 \cdot 10^{-29}$
5.	U2i3	$17 \cdot 10^{-18}$	66	66	$4.1 \cdot 10^8$	$5.5 \cdot 10^{-12}$	$4.00 \cdot 10^{-29}$
6.	R4j5	$16 \cdot 10^{-18}$	55	50	$4.8 \cdot 10^8$	$9.6 \cdot 10^{-12}$	$3.00 \cdot 10^{-29}$
7.	E3k4	$19 \cdot 10^{-18}$	75	60	$5.0 \cdot 10^8$	$6.0 \cdot 10^{-12}$	$2.00 \cdot 10^{-29}$
8.	G1l1	$14 \cdot 10^{-18}$	60	40	$2.0 \cdot 10^8$	$3.0 \cdot 10^{-12}$	$4.00 \cdot 10^{-29}$
9.	P5i3	$15 \cdot 10^{-18}$	60	50	$3.0 \cdot 10^8$	$2.0 \cdot 10^{-12}$	$4.00 \cdot 10^{-29}$
10.	T2s2	$14 \cdot 10^{-18}$	50	50	$2.0 \cdot 10^8$	$3.0 \cdot 10^{-12}$	$4.00 \cdot 10^{-29}$
11.	S2i3	$18 \cdot 10^{-18}$	60	55	$4.0 \cdot 10^8$	$7.0 \cdot 10^{-12}$	$3.00 \cdot 10^{-29}$
12.	R2r3	$11 \cdot 10^{-18}$	50	50	$4.0 \cdot 10^8$	$5.0 \cdot 10^{-12}$	$4.00 \cdot 10^{-29}$
13.	T2i3	$17 \cdot 10^{-18}$	65	45	$4.9 \cdot 10^8$	$1.0 \cdot 10^{-12}$	$4.50 \cdot 10^{-29}$
14.	Q1t1	$19 \cdot 10^{-18}$	50	40	$2.0 \cdot 10^8$	$3.0 \cdot 10^{-12}$	$4.00 \cdot 10^{-29}$
15.	O1k1	$17 \cdot 10^{-18}$	50	45	$4.0 \cdot 10^8$	$2.0 \cdot 10^{-12}$	$2.00 \cdot 10^{-29}$
16.	O2s2	$19 \cdot 10^{-18}$	50	45	$2.0 \cdot 10^8$	$4.0 \cdot 10^{-12}$	$2.00 \cdot 10^{-29}$

Table 3. Fourth model: computer simulation results (2) (Vasiliauskas et al., 2007)

The most precise match of laser characteristics was obtained for the laser with the characteristics shown in Fig. 13a (chirp and density of electrons; the chirp is proportional to the carrier density (Henry, 1982)) and Fig. 13b (optical power pulse characteristic).

Selected values for the matching of unknown parameters were: Γ = 0.55; R_1 = 0.041; R_2 = 0.661; τ_p = 1.5·10^{-12} s; α = 16.8·10^{-7} cm^3/s; β = 1·10^{-4}; N_0 = 24.3·10^{17} cm^{-3}; ε = 9.5·10^{-18}; τ_{j1} = 54·10^{-12} s; τ_{j2} = 50·10^{-12} s; A = 2.5·10^8 cm/s; B = 9.1·10^{-12} cm^3/s; C = 3.80·10^{-29} cm^6/s.

The values of parameters for other lasers, the comparison of simulation and experimental results are represented in Tables 1, 2 and 3. In order to evaluate the accuracy of simulation results the following parameters, such as the frequency (v) of relaxation oscillations, the time of oscillation decrement (T), "1" and "2" levels proportion (l) and the proportion of amplitude of first peak and level "1" (a) were compared (see Table 4). The averaged value of the mismatch (M) between the simulation and experimental results for these parameters was calculated (see Figs. 14 and 15).
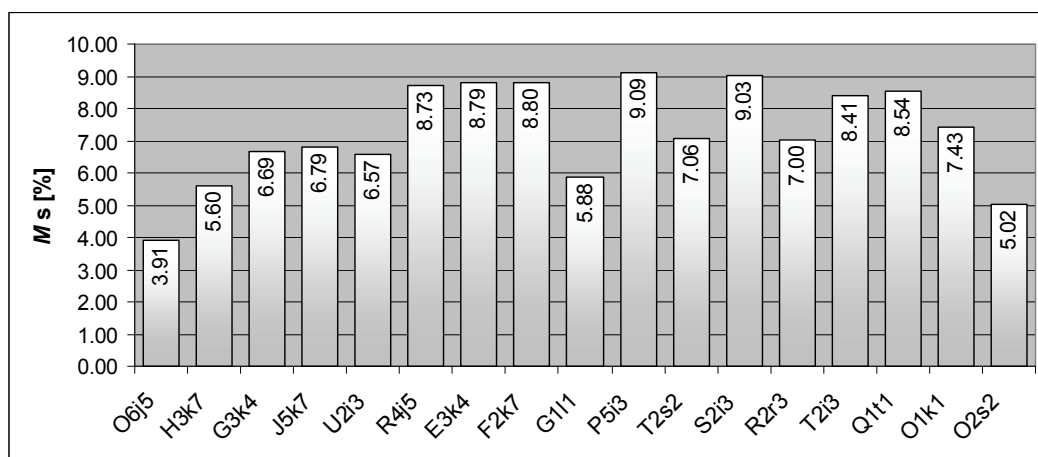

Fig. 14. Averaged value of the mismatch of simulated laser parameters for different lasers: Ms is for electron density characteristic (Vasiliauskas et al., 2007)
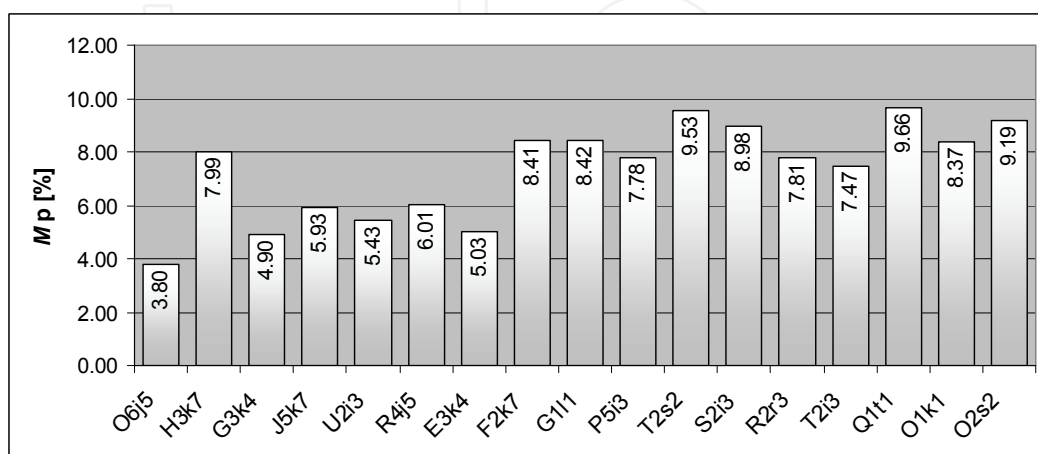

Fig. 15. Averaged value of the mismatch of simulated laser parameters for different lasers: Mp is for optical power characteristic (Vasiliauskas et al., 2007)

No.	DFB laser	Mismatch of simulation parameters [%]									
		v_s	v_p	T_s	T_p	l_s	l_p	a_s	a_p	M_s	M_p
1.	O6j5	2.33	2.02	8.60	7.43	1.33	4.85	3.39	0.90	3.91	3.80
2.	H3k7	1.35	7.44	9.72	9.90	9.61	7.33	1.74	7.29	5.60	7.99
3.	G3k4	1.49	5.38	9.84	8.22	9.36	4.08	6.04	1.92	6.69	4.90
4.	J5k7	2.14	9.98	9.97	8.25	8.37	4.50	6.67	0.98	6.79	5.93
5.	U2i3	0.90	4.81	9.75	9.84	9.62	3.94	6.02	3.12	6.57	5.43
6.	R4j5	9.32	6.56	9.84	9.21	6.40	6.20	9.35	2.08	8.73	6.01
7.	E3k4	5.51	4.96	9.87	9.76	9.85	2.19	9.93	3.19	8.79	5.03
8.	G1l1	3.43	8.01	9.78	9.97	1.59	8.96	8.72	6.74	5.88	8.42
9.	P5i3	6.59	9.89	9.97	9.68	9.89	4.57	9.93	6.98	9.09	7.78
10.	T2s2	9.82	9.33	9.43	9.71	2.89	9.83	6.11	9.26	7.06	9.53
11.	S2i3	8.07	7.97	9.51	9.75	9.09	8.92	9.43	9.28	9.03	8.98
12.	R2r3	9.96	9.91	6.64	8.74	1.79	3.59	9.62	8.99	7.00	7.81
13.	T2i3	9.65	9.82	8.60	9.09	9.63	6.67	5.77	4.30	8.41	7.47
14.	Q1t1	9.55	9.93	9.74	9.87	4.95	9.86	9.93	8.99	8.54	9.66
15.	O1k1	8.46	9.83	9.12	9.78	9.80	4.36	2.34	9.52	7.43	8.37
16.	O2s2	3.88	9.81	9.71	8.31	4.40	9.54	2.10	9.09	5.02	9.19

Table 4. Mismatch (%) of simulation data to experimental results (Vasiliauskas et al., 2007)

6. Conclusion

In this work the time-resolved frequency chirp characteristics under pulse operation of DFB LD were investigated. The optical beam carrier frequency (wavelength) deviations were measured by using a fiber Mach-Zehnder interferometer. The pulse current modulation at the 5 GHz and 1.25 GHz rate (10 Gbps and 2.5 Gbps) was achieved and the optical power and time-resolved frequency chirp pulses were investigated. LDs with a higher damping rate are preferable because of lower oscillation amplitudes at pulse edges, both for power pulses and for chirp pulses. It was found that at common operation conditions, i.e. average optical power P_w=5 mW and extinction ratio of 8.5 dB, the adiabatic chirp does not exceed 4.2-5.6 GHz and the transient chirp (amplitude of the first peak)- 3.2-10 GHz. To summarize, total chirp does not exceed 16 GHz. The chirp parameter (also known as the linewidth enhancement factor) was extracted from time-resolved frequency chirp measurements, which was found to be in the range of 2-2.8 for various devices.

The transient characteristics of semiconductor lasers were investigated. The unknown laser parameters which were not measured in the experiment were obtained by using computer simulation. Based on these simulation results a parameter estimation technique was suggested. The rate equations used for computer simulation were improved by including new terms which were not used in earlier simulations (Šermukšnis et al., 2004a, 2004b). Transient processes were simulated for a large number of similar DFB lasers. The best results were obtained by using the fourth physical model. The mismatch between the simulation and experimental results for all analyzed laser parameters in this case did not exceed the limit of 10%.

7. References

Agrawal, G.P. & Dutta, N.K. (1993). *Semiconductor Lasers, 2nd Edition*, Van Nostarnd Reinhold Co., ISBN 0-442-01102-4, New York, USA

Agrawal, G.P. (2002). *Fiber-Optic Communication Systems, 3nd Edition,* John Wiley & Sons, Inc., ISBN 0-471-21571-6, New York, USA.

Alder, T.; Stohr, A.; Heinzelmann, R. & Jager, D. (2000). High-Efficiency Fiber-to-Chip Coupling Using Low-Loss Tapered Single-Mode Fiber. *IEEE Photonics Technology Letters,* Vol.12, No.8, (August 2000), pp. 1016-1018, ISSN 1041-1135

Arakawa, Y. & Yariv, A. (1985). Fermi energy dependence of linewidth enhancement factor of GaAlAs buried heterostructure lasers. *Applied Physics Lett*ers, Vol.47, No.9, (November 1985), pp. 905-907, ISSN 0003-6951

Bergano, N. S. (1988). Wavelenght discriminator method for measuring dynamic chirp in DFB lasers. *Electronics Lett*ers, Vol.24, No.20 (September 1988), pp. 1296-1297, ISSN 0013-5194

Bhattacharya, P; Klotzkin, D.; Qasaimeh, O.; Zhou, W.; Krishna, S. & Zhu, D. (2000). High-Speed Modulation and Switching Characteristics of In(Ga)As-Al(Ga)As Self-Organized Quantum-Dot Lasers. *IEEE Journal of Selected Topics in Quantum Electronics,* Vol. 6, No. 3, (May 2000), pp. 426-438, ISSN 1077-260X.

Carroll, J.E.; Whiteaway, J.E.A. & Plumb, R.G.S. (1998). *Distributed feedback semiconductors lasers (IEE Circuits, Devices and Systems)*, IEE, ISBN 0852969171, London, UK

Fukuda, M. (1999). *Optical semiconductor devices*, John Wiley & Sons, ISBN 978-0-471-14959-0, New York, USA

Harder, C.; Vahala, K. & Yariv, A. (1983). Measurement of the linewidth enhancement factor α of semiconductor lasers. *Applied Physics Lett*ers, Vol.42, No.4 (February 1983), pp. 328-330, ISSN 0003-6951

Henry, C.H. (1982). Theory of the line width of semiconductor lasers. *IEEE Journal of Quantum Electroni*cs, Vol.18, No.2, (February 1982), pp. 259-264, ISSN 0018-9197

Henry, C. H. (1983). Theory of the Phase Noise and Power Spectrum of a Single Mode Injection Laser. *IEEE Journal of Quantum Electronics,* Vol.19, No.9, (September 1983), pp. 1391-1397, ISSN 0018-9197

Henry, C. H. (1986). Phase Noise in Semiconductor Lasers. *IEEE Journal of Lightwave Technology,* Vol.4, No.3, (March 1986), pp. 298-311, ISSN 0733-8724

Jeong, J. & Park, Y. K. (1997). Accurate Determination of Transient Chirp Parameter in High Speed Digital Lightwave Transmitters. *Electronics Letters,* Vol.33, No.7, (March 1997) pp. 605-606, ISSN 0013-5194

Kikuchi, K. & Okoshi, T. (1985). Estimation of linewidth enhancement factor of AlGaAs lasers by correlation measurement between FM and AM noises. *IEEE Journal of Quantum Electroni*cs, Vol.21, No.6 (June 1985), pp. 669 - 673, ISSN 0018-9197

Kikuchi, K.; Okoshi, T. & Kawai, T. (1984). Estimation of linewidth enhancement factor α of CSP-type AlGaAs lasers from measured correlation between AM and FM noises. *Electronics Lett*ers, Vol.20, No.11 (May 1984), pp. 450-451, ISSN 0013-5194

Kikuchi, K. (1990). Static Frequency Chirping in λ/4-Phase-Shifted Distributed-Feedback Semiconductor Lasers: Influence of Carrier-Density Nonuniformity Due to Spatial Hole Burning. *IEEE Journal of Quantum Electronics,* Vol.26, No.1, (January 1990), pp. 45-49, ISSN 0018-9197

Koyama, F. & Suematsu, Y. (1985). Analysis of Dynamic Spectral Width of Dynamic-Single-Mode (DSM) Lasers and Related Transmission Bandwidth of Single-Mode. *IEEE Journal of Quantum Electronics,* Vol.21, No.4, (April 1985), pp. 292-297, ISSN 0018-9197

Larsson, A.; Carlsson, C.; Gustavsson, J.; Haglund, A; Modh, P. & Bengtsson, J. (2004). Direct High-Frequency Modulation of VCSELs and Applications in Fibre Optic RF and Microwave Links. *New Journal of Physics,* Vol. 6, No. 1, (November 2004), pp. 1-17, ISSN 1367-2630

Laverdiere, C.; Fekecs, A. & Tetu, M. A. (2003). New Method for Measuring Time-Resolved Frequency Chirp of High Bit Rate Source. *IEEE Photonics Technology Letters,* Vol.15, No.3, (March 2003), pp. 446-448, ISSN 1041-1135

Linke, R. A. (1985). Modulation Induced Transient Chirping in Single Frequency Lasers. *IEEE Journal of Quantum Electronics,* Vol.21, No. 6, (June 1985), pp. 593-597, ISSN 0018-9197

Lu, H.; Makino T. B & Li, G. P. (1995). Dynamic Properties of Partly Gain-Coupled 1.55-µm DFB Lasers. *IEEE Journal of Quantum Electronics,* Vol. 31, No. 8, (August 1995), pp. 1443-1995, ISSN 0018-9197

Olsen, C. M. & Lin, C. (1989). Time-Resolved Chirp Evaluations of Gbit/s NRZ and Gain-Switched DFB Laser Pulses Using Narrowband Fabry-Perot Spectrometer. *Electronics Letters,* Vol.25, No.16, (August 1989), pp. 1018-1019, ISSN 0013-5194

Saunders, R. A.; King, J. P. & Hardcastle, I. (1994). Wideband Chirp Measurement Technique for High Bit Rate Sources. *Electronics Letters,* Vol.30, No16, (August 1994), pp. 1336-1338, ISSN 0013-5194

Shani, Y.; Henry, C. H.; Kistler, R. C.; Orlowski, K. J. & Ackerman, D. A. (1989). Efficient Coupling of a Semiconductor Laser to an Optical Fiber by Means of a Tapered Waveguide on Silicon. *Applied Physics Letters,* Vol. 55, No.23 (December 1989), pp. 2389-2391, ISSN 0003-6951

Šermukšnis, E.; Vyšniauskas, J.; Vasiliauskas, T. & Palenskis, V. (2004a). Computer Simulation of High Frequency Modulation of Laser Diode Radiation. *Lithuanian Journal of Physics*, Vol. 44, No.6, (December 2004), pp. 415-420, ISSN 1648-8504

Šermukšnis, E.; Vyšniauskas, J.; Palenskis, V.; Matukas, J. & Pralgauskaitė, S. (2004b). Dynamic characteristics of gain-coupled InGaAsP laser diodes and their reliability. *Kwartalnik elektroniki i telekomunikacji*, Vol.50, No.4, (April 2004), pp. 591-603, ISSN 0867-6747

Šermuksnis, E.; Vyšniauskas, J. & Palenskis, V. (2005). Dynamic characteristics and reliability of gain-coupled InGaAsP laser diodes. *Proceedings of SPIE, Optical Materials and Applications*, Vol.5946, No.8, (August 2005), pp. 300-308, ISBN 9780819459534

Tammela, S.; Ludvigsen, H. & Kaivola, M. (1997). Time-Resolved Frequency Chirp Measurement Using a Silicon-Wafer Etalon. *IEEE Photonics Technology Letters,* Vol.9, No.4, (April 1997), pp. 475-477, ISSN 1041-1135

Tatham, M. C.; Lealman, I. F.; Seltzer, C. P.; Westbrook, L. D. & Cooper, D. M. (1992). Resonance frequency, damping, and differential gain in 1.5 µm multiple quantum-well lasers. *IEEE Journal of Quantum Electronics,* Vol. 28, No.2, (February 1992), pp. 408-414, ISSN 0018-9197

Vasiliauskas, T.; Butkus, V.; Šermukšnis, E.; Palenskis, V. & Vyšniauskas, J. (2007). Computer Simulation of Transient Processes in DBF Semiconductor Lasers. *Lithuanian Journal of Physics*, Vol. 47, No.4, (December 2007), pp. 397-402, ISSN 1648-8504

Welford, D. A. (1985). Rate Equation Analysis for the Frequency Chirp to Modulated Power Ratio of a Semiconductor Diode Laser. *IEEE Journal of Quantum Electronics,* Vol.21, No.11, (November 1985), pp. 1749-1751, ISSN 0018-9197
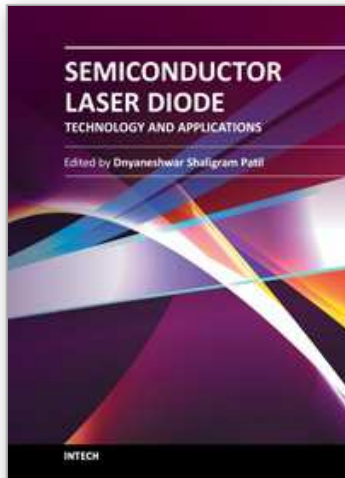
Semiconductor Laser Diode Technology and Applications

Edited by Dr. Dnyaneshwar Shaligram Patil

This book represents a unique collection of the latest developments in the rapidly developing world of semiconductor laser diode technology and applications. An international group of distinguished contributors have covered particular aspects and the book includes optimization of semiconductor laser diode parameters for fascinating applications. This collection of chapters will be of considerable interest to engineers, scientists, technologists and physicists working in research and development in the field of semiconductor laser diode, as well as to young researchers who are at the beginning of their career.

How to reference

In order to correctly reference this scholarly work, feel free to copy and paste the following:

Juozas Vysniauskas, Tomas Vasiliauskas, Emilis Sermuksnis, Vilius Palenskis and Jonas Matukas (2012). Investigation of High-Speed Transient Processes and Parameter Extraction of InGaAsP Laser Diodes, Semiconductor Laser Diode Technology and Applications, Dr. Dnyaneshwar Shaligram Patil (Ed.), ISBN: 978-953-51-0549-7, InTech, Available from: http://www.intechopen.com/books/semiconductor-laser-diode-technology-and-applications/investigation-of-high-speed-transient-processes-and-parameter-extraction-of-ingaasp-laser-diodes

INTECH
open science | open minds